

tions to telomeric silencing, and indicate that the role of histones located elsewhere in chromosomes is gene specific rather than generally repressive. Knowledge of the effect of histone depletion on expression of all yeast genes provides the framework for future studies to identify the complete set of factors that are responsible for telomere-proximal silencing, and establishes the foundation for accurately reconstituting gene-specific transcription reactions *in vitro*. □

Methods

Strains, media and growth conditions

S. cerevisiae UKY403 (ref. 15; histone H4 depletion) and MHY308 (ref. 15; wild-type histone H4) cells were grown in parallel in galactose-containing medium (YEPGalactose) and switched to glucose-containing medium (YPD). Cells were grown for various times (0, 0.5, 1, 1.5, 2, 4, 6 h) in YPD before harvesting. The final OD₆₀₀ for all time points was 0.5–0.7. All other strains were grown in YPD media until reaching OD₆₀₀ = 0.5–0.7 (see authors' Web site for more details and a complete list of all strains used).

Genome-wide expression profiling

Biotin-labelled cRNA target was prepared as described²². The cRNA was hybridized to a set of four oligonucleotide arrays (GeneChip Ye6100 arrays, Affymetrix) and scanned as described¹⁶. Intensities were captured using GeneChip software (Affymetrix) and a single raw expression level for each gene was determined.

Data analysis

The raw data from each chip were normalized and corrected as described²². A change in mRNA levels was deemed significant and reported in the lists of genes whose expression was increased or decreased more than 3-fold based on the following criteria: the average fold change was more than 3-fold, the fold change in each experiment was greater than 1.5-fold and the change in the values was above background values in both comparisons. See authors' Web site for more details.

Telomere-proximal gene analysis and statistics

Genes within 40 kb of a telomere throughout the genome were pooled and ordered according to their distance from a telomere. Genes with sequence homologues whose mRNA levels could not be distinguished with certainty (genes with an Affymetrix 'f' call) were excluded from the analysis. The genes were grouped by their distance from a telomere either in consecutive intervals of 50 genes (Table 1) or in a sliding 50-gene window which was moved in 10-gene steps (Fig. 4a). For each interval, the fraction of genes that were depressed in each mutant was calculated. The change in the fraction of genes that were depressed with distance from telomere is shown in Fig. 4a. A χ^2 value for each interval was calculated by comparing the fraction of genes that were de-repressed in the interval to the genome-wide average (Table 1).

Received 16 July; accepted 6 September 1999.

1. Paranjape, S. M., Kamakaka, R. T. & Kadonaga, J. T. Role of chromatin structure in the regulation of transcription by RNA polymerase II. *Annu. Rev. Biochem.* **63**, 265–297 (1994).
2. Workman, J. L. & Kingston, R. E. Alteration of nucleosome structure as a mechanism of transcriptional regulation. *Annu. Rev. Biochem.* **67**, 545–579 (1998).
3. Gregory, P. D. & Horz, W. Life with nucleosomes: chromatin remodelling in gene regulation. *Curr. Opin. Cell Biol.* **10**, 339–345 (1998).
4. Aparicio, O. M., Billington, B. L. & Gottschling, D. E. Modifiers of position effect are shared between telomeric and silent mating-type loci in *S. cerevisiae*. *Cell* **66**, 1279–1287 (1991).
5. Kurtz, S. & Shore, D. RAP1 protein activates and silences transcription of mating-type genes in yeast. *Genes Dev.* **5**, 616–628 (1991).
6. Kyrion, G., Liu, K., Kiu, C. & Lustig, A. J. RAP1 and telomere structure regulate telomere position effects in *Saccharomyces cerevisiae*. *Genes Dev.* **7**, 1146–1159 (1993).
7. Loo, S. & Rine, J. Silencing and heritable domains of gene expression. *Annu. Rev. Cell. Dev. Biol.* **11**, 519–548 (1995).
8. Zakian, V. A. Structure, function, and replication of *Saccharomyces cerevisiae* telomeres. *Annu. Rev. Genet.* **30**, 141–172 (1996).
9. Grunstein, M. Yeast heterochromatin: regulation of its assembly and inheritance by histones. *Cell* **93**, 325–328 (1998).
10. Lustig, A. J. Mechanisms of silencing in *Saccharomyces cerevisiae*. *Curr. Opin. Genet. Dev.* **8**, 233–239 (1998).
11. Hecht, A., Strahl-Bolsinger, S. & Grunstein, M. Spreading of transcriptional repressor SIR3 from telomeric heterochromatin. *Nature* **383**, 92–96 (1996).
12. Strahl-Bolsinger, S., Hecht, A., Luo, K. & Grunstein, M. SIR2 and SIR4 interactions differ in core and extended telomeric heterochromatin in yeast. *Genes Dev.* **11**, 83–93 (1997).
13. Han, M. & Grunstein, M. Nucleosome loss activates yeast downstream promoters *in vivo*. *Cell* **55**, 1137–1145 (1988).
14. Han, M., Kim, U. J., Kayne, P. & Grunstein, M. Depletion of histone H4 and nucleosomes activates the PHO5 gene in *Saccharomyces cerevisiae*. *EMBO J.* **7**, 2221–2228 (1988).
15. Kim, U. J., Han, M., Kayne, P. & Grunstein, M. Effects of histone H4 depletion on the cell cycle and transcription of *Saccharomyces cerevisiae*. *EMBO J.* **7**, 2211–2219 (1988).
16. Wodicka, L., Dong, H., Mittmann, M., Ho, M. H. & Lockhart, D. J. Genome-wide expression monitoring in *Saccharomyces cerevisiae*. *Nature Biotechnol.* **15**, 1359–1367 (1997).
17. Saunders, M. J., Yeh, E., Grunstein, M. & Bloom, K. Nucleosome depletion alters the chromatin structure of *Saccharomyces cerevisiae* centromeres. *Mol. Cell Biol.* **10**, 5721–5727 (1990).

18. Chavez, S. & Beato, M. Nucleosome-mediated synergism between transcription factors on the mouse mammary tumor virus promoter. *Proc. Natl Acad. Sci. USA* **94**, 2885–2980 (1997).
19. DeRisi, J. L., Iyer, V. R. & Brown, P. O. Exploring the metabolic and genetic control of gene expression of a genomic scale. *Science* **278**, 680–686 (1997).
20. Schild, C., Claret, F. X., Wahli, W. & Wolffe, A. P. A nucleosome-dependent static loop potentiates estrogen-regulated transcription from the *Xenopus* vitellogenin B1 promoter *in vitro*. *EMBO J.* **12**, 423–433 (1993).
21. Shen, X. & Gorovsky, M. A. Linker histone H1 regulates specific gene expression but not global transcription *in vivo*. *Cell* **86**, 475–483 (1996).
22. Holstege, F. C. *et al.* Dissecting the regulatory circuitry of a eukaryotic genome. *Cell* **95**, 717–728 (1998).
23. Moretti, P., Freeman, K., Coddly, L. & Shore, D. Evidence that a complex of SIR proteins interacts with the silencer and telomere-binding protein RAP1. *Genes Dev.* **8**, 2257–2269 (1994).
24. Rine, J. & Herskowitz, I. Four genes responsible for a position effect on expression from HML and HMR in *Saccharomyces cerevisiae*. *Genetics* **116**, 9–22 (1987).
25. Enomoto, S., McCune-Zierath, P. D., Gerami-Nejad, M., Sanders, M. A. & Berman, J. RLF2, a subunit of yeast chromatin assembly factor-I, is required for telomeric chromatin function *in vivo*. *Genes Dev.* **11**, 358–370 (1997).
26. Kaufman, P. D., Kobayashi, R. & Stillman, B. Ultraviolet radiation sensitivity and reduction of telomeric silencing in *Saccharomyces cerevisiae* cells lacking chromatin assembly factor-I. *Genes Dev.* **11**, 345–357 (1997).
27. Laroche, T. *et al.* Mutation of yeast Ku genes disrupts the subnuclear organization of telomeres. *Curr. Biol.* **8**, 653–656 (1998).
28. Brachmann, C. B. *et al.* The SIR2 gene family, conserved from bacteria to humans, functions in silencing, cell cycle progression, and chromosome stability. *Genes Dev.* **9**, 2888–2902 (1995).
29. Nislow, C., Ray, E. & Pillus, L. SET1, a yeast member of the trithorax family, functions in transcriptional silencing and diverse cellular processes. *Mol. Biol. Cell* **8**, 2421–2436 (1997).
30. Eisen, M. B., Spellman, P. T., Brown, P. O. & Botstein, D. Cluster analysis and display of genome-wide expression patterns. *Proc. Natl Acad. Sci. USA* **95**, 14863–14969 (1998).

Supplementary Information is available on Nature's World-Wide Web site (<http://www.nature.com>) or as paper copy from the London editorial office of Nature.

Acknowledgements

We thank T. Golub, D. Gottschling, C. Hengartner, T. Lee, H. Madhani and C. Wilson for helpful discussions, and N. Hannett, M. Gaasenbeek and C. Huard for technical support. This work was supported by funds from the NIH, Bristol-Myers Squibb Company, Affymetrix Inc., Millennium Pharmaceuticals Inc., and the Whitehead Institute Leadership Circle. J.J.W. is a predoctoral fellow of the National Science Foundation, F.C.P.H. was supported by fellowships from EMBO and the Hujan Frontier Science Program and E.G.J. is a predoctoral fellow of the Howard Hughes Medical Institute.

Correspondence and requests for materials should be addressed to R.A.Y. (e-mail: young@wi.mit.edu).

LTP promotes formation of multiple spine synapses between a single axon terminal and a dendrite

N. Toni*, P.-A. Buchs*, I. Nikonenko*, C. R. Bron† & D. Muller*

* *Neuropharmacology, CMU, University of Geneva, 1211 Geneva 4, Switzerland*
 † *Institute of Anatomy, University of Bern, 3000 Bern, Switzerland*

Structural remodelling of synapses^{1–4} and formation of new synaptic contacts^{5–8} has been postulated as a possible mechanism underlying the late phase of long-term potentiation (LTP), a form of plasticity which is involved in learning and memory⁹. Here we use electron microscopy to analyse the morphology of synapses activated by high-frequency stimulation and identified by accumulated calcium in dendritic spines. LTP induction resulted in a sequence of morphological changes consisting of a transient remodelling of the postsynaptic membrane followed by a marked increase in the proportion of axon terminals contacting two or more dendritic spines. Three-dimensional reconstruction revealed that these spines arose from the same dendrite. As pharmacological blockade of LTP prevented these morphological changes, we conclude that LTP is associated with the formation of new, mature and probably functional synapses contacting the same presynaptic terminal and thereby duplicating activated synapses.

Electron microscopic analyses of the morphological changes associated with LTP are difficult without being able to identify activated synapses¹⁰. Here we used a potassium chromium–trisoxalate precipitation protocol during osmium fixation¹¹ to reveal, as a fine precipitate, the calcium that had accumulated in dendritic spines following high-frequency stimulation (Fig. 1a). Previous work had shown that this method is specific for calcium, that the precipitate is only present in a small proportion of spine profiles under control conditions, and that theta burst stimulation (TBS) to a group of CA3 neurons results in an NMDA (*N*-methyl-D-aspartate)-dependent increase in the number of CA1 spine profiles containing calcium precipitate⁴ (Fig. 1b). Analysis of the density of precipitate in spine profiles (Fig. 1c) shows a bimodal distribution with a clear distinction between labelled (black columns) and unlabelled (grey columns) profiles. The small number of profiles for which classification was unclear (white column, 1–2% of profiles) were discarded from quantitative analyses.

Using this approach, we examined the ultrastructural correlate of LTP as a function of time after induction of synaptic potentiation. LTP was induced at a group of synapses by application of TBS and their responses were monitored over various periods of time (5, 15, 30, 45, 60 and 120 min). A second TBS was applied 5 min before fixation to re-label the same synapses with calcium precipitate (Fig. 1d). The first notable change observed

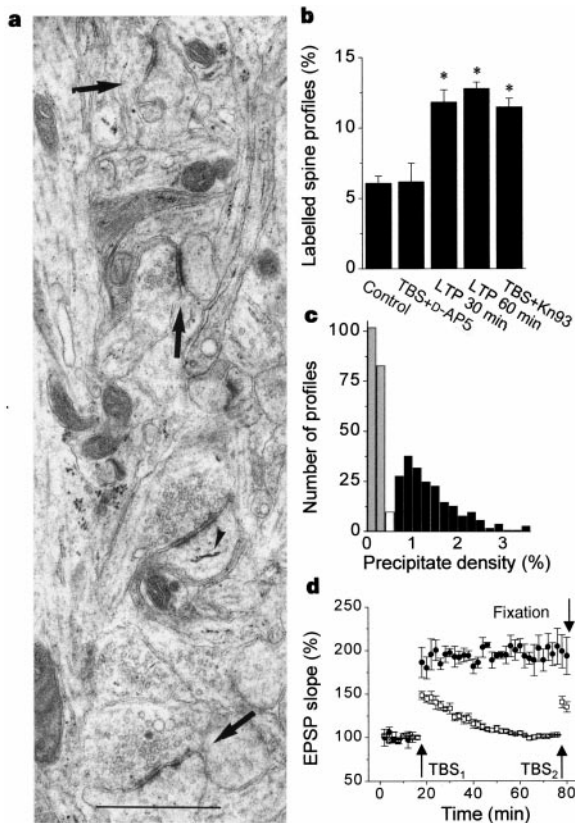


Figure 1 Labelling of activated spine profiles by induction of LTP. **a**, Low-magnification view of synaptic profiles in a slice culture fixed 5 min after high-frequency stimulation showing one labelled (arrowhead on labelling) and three unlabelled (arrows) spine profiles. Scale bar, 1 μ m. **b**, Proportion of spine profiles containing calcium precipitate under the various conditions tested (asterisk, $P < 0.001$). **c**, Distribution of the precipitate density, expressed in per cent and measured as the area of precipitate over the spine profile area, for the 60-min time point. Note the distinction between the populations of labelled (black columns) and unlabelled (grey columns) profiles. Profiles for which classification was unclear (white column) were discarded. **d**, Electrophysiological recordings of the LTP induced in control organotypic cultures (black circles) and following treatment with the kinase antagonist KN93 (open squares). After LTP induction (TBS_1), a second TBS was applied 5 min before fixation to re-label activated synapses.

in the population of labelled dendritic spines was an increase in the proportion of spine profiles having a partitioned postsynaptic density (PSD), also referred to as perforated synapses^{1–4,10,11} (Fig. 2a, b). The proportion of perforated synapses was $18.8 \pm 1\%$ in non-stimulated cultures; it increased gradually to $23.4 \pm 3.5\%$, $25 \pm 2.4\%$ and $45.8 \pm 2.8\%$ of all labelled synaptic profiles at 5, 15 and 30 min after stimulation, respectively ($n = 3–7$; 220–949 spine profiles analysed). Unexpectedly, the occurrence of these perforated synapses was only transient: their proportion decreased to $28.6 \pm 7.7\%$ after 45 min to reach control values after 60 min ($18.1 \pm 2.5\%$). Unbiased stereological measurements confirmed these changes ($15 \pm 2\%$, $38 \pm 2\%$ and $15 \pm 5\%$ at 5, 30 and 60 min, respectively; $n = 2$; 65–112 spine profiles). These changes were not detected when non-labelled synapses were analysed ($22.7 \pm 1.1\%$, $n = 6$, 246 spine profiles), and were accompanied by transitory changes in the perforation characteristics of the synapses. Figure 2e shows that the size of the perforation and of the spinule, characterized by a small protrusion of the postsynaptic membrane into the presynaptic terminal (Fig. 2f), was considerably greater 30 min after stimulation than at other time points (perforation size: 284 ± 29 nm at 30 min versus 157 ± 19 nm and 145 ± 14 nm at 0–15 min and 45–120 min, respectively, $n = 5–8$; spinule height: 167 ± 28 nm versus 62 ± 4 nm and 74 ± 5 nm; $n = 5–11$).

These transitory changes were followed, one hour after stimulation, by a threefold increase in the presence of multiple spine boutons (Fig. 2c, d). These were characterized by the presence of at least two dendritic spines contacting the same axon terminal. Under control conditions, when analysing non-stimulated slices,

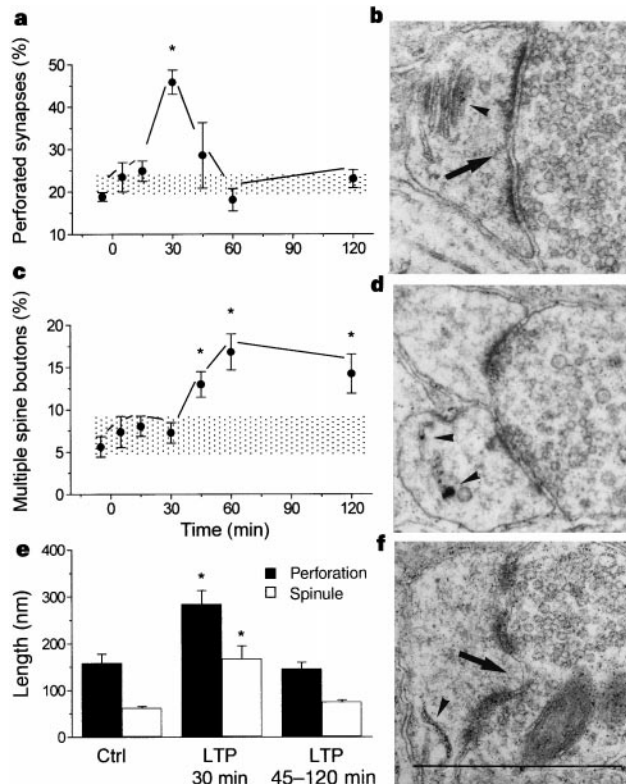


Figure 2 Time course of ultrastructural changes associated with LTP induction. **a**, Transient changes in the proportion of perforated synapses ($n = 3–7$; 220–630 spine profiles; asterisk, $P < 0.001$). **b**, A perforated spine profile (arrow, perforation). **c**, Increase in the proportion of multiple spine boutons 45–60 min after LTP induction ($n = 3–7$; 206–364 spine profiles; asterisk, $P < 0.01$). **d**, A multiple spine bouton. **e**, Morphometric changes in the size of the perforation and spinule after LTP induction ($n = 5–11$; 65–149 spine profiles; asterisk, $P < 0.01$). **f**, A perforated synapse exhibiting a prominent spinule (arrow). Calcium precipitates indicated by arrowheads. Scale bar, 1 μ m.

the proportion of multiple spine boutons was $5.6 \pm 1.2\%$ of labelled spine profiles. Similar values were found 5, 15 and 30 min after high frequency stimulation ($7.3 \pm 1.8\%$, $8 \pm 1.2\%$ and $7.3 \pm 1.2\%$, respectively; $n = 3-7$; 206-364 spine profiles). However, 45 min after LTP induction, the proportion of labelled, multiple spine boutons in which either one or both spine profiles contained the precipitate represented $13 \pm 1.5\%$ of all labelled spine profiles. This value reached $16.8 \pm 2.1\%$ 1 h after LTP induction and $14.2 \pm 2.3\%$ after 2 h ($n = 3-4$, 223-308 spine profiles). No increase was detected when analysing non-labelled synapses ($5.9 \pm 0.7\%$ 60 min after LTP, $n = 3$, 323 spine profiles).

We used unbiased stereological methods to confirm these results. Analyses were made 5 and 60 min after LTP induction and showed the same increase in multiple spine boutons (5 min: $6.2 \pm 0.4\%$, $n = 2$, 64 spine profiles; 60 min: $15 \pm 2.5\%$, $n = 2$, 119 spine profiles). In addition, to establish further the link between LTP induction and these morphological changes, we carried out experiments in which LTP was pharmacologically blocked by treatment with the calcium/calmodulin protein kinase II antagonist KN93 (Fig. 1d). Labelling of spine profiles was not affected by KN93 treatment (Fig. 1b), but we did not detect any increase in perforated synapses or in multiple spine boutons 30 and 60 min after stimulation, respectively (Fig. 3). These data indicate that the morphological changes reported here are specifically associated with induction of LTP.

As the increase in multiple spine boutons indicated possible synaptogenesis, we used three-dimensional reconstruction of 75 multiple spine boutons to analyse the origins of the newly formed dendritic spines (Fig. 4). Analysis of unlabelled multiple spine boutons reconstructed 5, 45 and 60 min after stimulation revealed, in agreement with previous studies¹², that in $89 \pm 8\%$ of cases the two spines arose from different dendrites (mean \pm s.e.m. of six cultures, but 38 out of 41 reconstructed boutons; Fig. 4a, b). A similar result was found when analysing labelled multiple spine boutons reconstructed from a slice culture fixed 5 min after stimulation (spines arose from different dendrites in eight out of nine cases). In contrast, however, reconstruction of 25 labelled multiple spine boutons from four cultures fixed 45-60 min after LTP induction revealed that in 15 of them the two spines arose from the same dendrite. The mean proportion of multiple spine boutons in which

the two spines arose from the same dendrite was thus $66 \pm 14\%$ in four cultures as compared to $11 \pm 8\%$ for unlabelled multiple spine boutons ($n = 6$; $P < 0.01$). As shown in Fig. 4a, the increase in multiple spine boutons measured on single sections essentially resulted from cases in which the two spines arose from the same dendrite (Fig. 4c-e). This new population of duplicated synapses thus clearly indicated that new synapses were being formed between the same axon terminal and dendrite.

The morphology of these newly formed spines was similar to that of mature dendritic spines (Fig. 4e). They had well defined necks and spine heads, sometimes including a spine apparatus, and a clearly visible PSD facing a pool of presynaptic vesicles. Furthermore, for the labelled multiple spine boutons observed after 45-60 min and contacting spines originating from the same dendrite, serial section analysis indicated that in 9 out of 15 cases calcium precipitate was clearly visible in both spines. Such cases were also frequently observed on single section analyses, indicating that a significant fraction of the new spine synapses formed 1 h after LTP induction probably made mature and functional synapses.

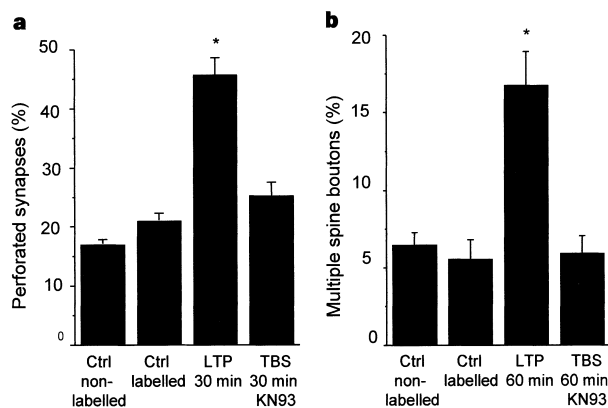


Figure 3 Blockade of LTP prevents morphological changes. **a**, Proportion of perforated spine profiles observed under control (ctrl) conditions (labelled and unlabelled spine profiles in non-stimulated cultures ($n = 3-4$, 319-630 spine profiles)), 30 min after LTP induction ($n = 4$, 358 spine profiles) and following high-frequency stimulation in the presence of $10 \mu\text{M}$ KN93 ($n = 4$, 313 spine profiles). **b**, Proportion of multiple spine boutons under control conditions (labelled and unlabelled spine profiles in non-stimulated cultures ($n = 3-4$, 319-630 spine profiles)), 60 min after LTP induction ($n = 4$, 308 spine profiles) and following high-frequency stimulation in the presence of $10 \mu\text{M}$ KN93 ($n = 3$, 183 spine profiles). The changes in both perforated synapses and multiple spine boutons were blocked by KN93 treatment (asterisk, $P < 0.001$ and $P < 0.01$, respectively).

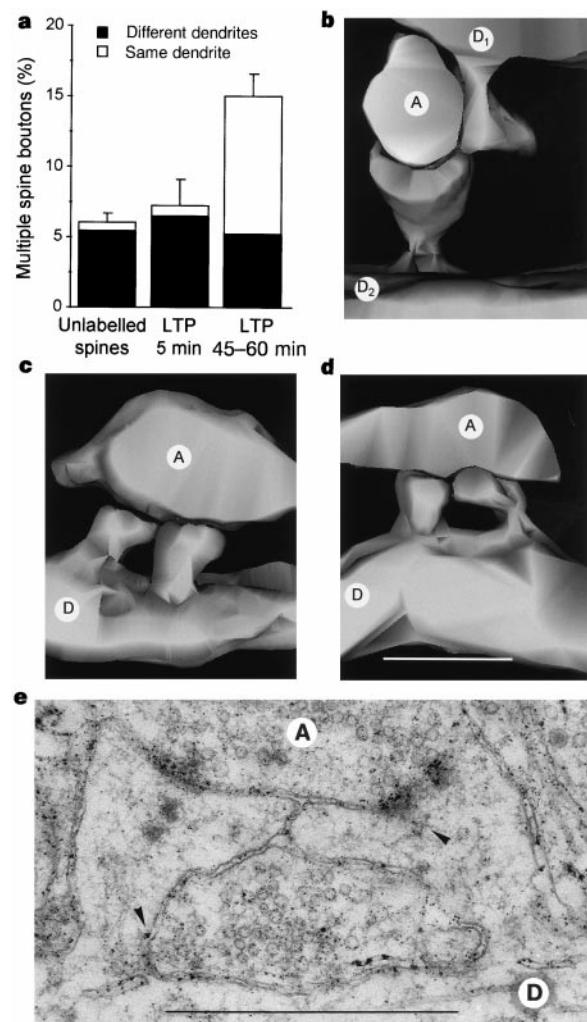


Figure 4 Three-dimensional reconstruction of multiple spine boutons. **a**, Proportion of multiple spine boutons measured on single sections. For each column, we calculated from three-dimensional reconstruction the proportion of boutons in which the two spines arose from different dendrites (black) or the same (white) dendrite (see text for numbers and proportions). **b**, A reconstructed, unlabelled multiple spine bouton in which the two spines arise from different dendrites. **c, d**, Labelled, multiple spine boutons observed 60 min after LTP induction in which the two spines arise from the same dendrite. Axons are indicated by A and dendrites by D. **e**, Two spines originating from the same dendrite (arrowheads: precipitate, unfortunately mainly present on another section). Scale bars, $1 \mu\text{m}$.

By using a calcium precipitation method to identify a subset of synapses likely to represent activated synapses, we have provided strong evidence that the late phase of LTP is associated with the formation of new, mature and functional spine synapses contacting the same presynaptic terminals.

One potential source of error in this study may come from selection biases. The calcium precipitate is primarily associated with smooth endoplasmic reticulum-like structures which are unevenly distributed among different types of synapse¹³. Furthermore, activity-dependent changes in the size of the spine head, PSD, perforation or smooth endoplasmic reticulum may affect quantitative results and particularly estimates of the proportion of perforated synapses^{1,2}. However, it seems unlikely that these possible biases would have modified our main conclusions. First, all data were obtained by analysing at different times the same population of synapses (labelled spine profiles), and strong evidence suggests that these mainly represented activated synapses⁴. Second, our main finding, the increase in the proportion of multiple spine boutons 60 min after LTP induction, was observed using single-section analyses, unbiased stereological methods and three-dimensional reconstruction. Third, these morphological changes were time-dependent and thus unrelated to the protocol used. Fourth, they were prevented by pharmacological blockade of LTP and thus are specifically associated with LTP. Finally, our conclusions are consistent with the results of many other studies^{5,6,14} and in particular with the demonstration by confocal microscopy of the occurrence of dendritic protrusions and spine-like structures following LTP induction^{7,8}.

An important finding added by the present study is that the new spines appearing after LTP induction include adjacent, mature synapses that contact the same presynaptic terminal. Note, however, that spine density was not directly assessed here and that new spines that do not share the same presynaptic bouton would not have been detected. These data nevertheless indicate that LTP may include duplication of synaptic contacts between an activated axon and a dendrite. Furthermore, the analysis of the presence of calcium precipitates in the spines arising from the same dendrite indicates that at least some of these newly formed synapses were functional. This mechanism could thus contribute to the stability of LTP and at the same time account for its synapse-specificity. From a quantitative point of view, our data indicate that newly formed synapses could represent up to 20% of stimulated synapses. This value is likely to be an underestimate, as newly formed synapses not sharing the same presynaptic bouton could not be detected.

Could new synapses have also been formed with other non-stimulated axon terminals? The increase in multiple spine boutons observed following LTP induction only concerned labelled spines and not unlabelled spines. Furthermore, we did not detect any increase in multiple spine boutons in which the two spines arose from different dendrites (the only situation which could eventually have reflected nonspecific synaptogenesis). Other studies, however, will be required to clarify this point.

The time course of the morphological changes is also of interest. The multiple spine boutons reported here were first detected 45–60 min after induction, a time course which is consistent with the occurrence of the new spines observed by Engert and Bonhoeffer⁷. Maletic-Savatic *et al.*⁸, however, reported a rapid occurrence of dendritic protrusions (within a few minutes) following high-frequency stimulation. We did not find such changes, although only structures defined by a clearly identified postsynaptic density were analysed. They could have thus remained undetected if the dendritic protrusions observed rapidly after stimulation did not exhibit all features of mature synapses^{15,16}. The most rapid change observed here was a transient increase in perforated synapses. How this morphological change relates to the dendritic protrusions and the subsequent formation of multiple spine boutons remains unclear^{10,17}. Perforated synapses could represent an intermediate step in the process of synapse formation and spine splitting^{18,19}. They

could also simply reflect the membrane dynamics and receptor turnover occurring at that time at activated synapses^{20–22}. It is of interest that the sequence of events reported here at the ultrastructural level coincides with the changes reported to occur with synapse turnover and formation of new synaptic contacts in several other *in vitro* models^{18,19,23,24}.

Together, these results indicate that the late phase of LTP is likely to be associated with the formation of new and possibly functional synapses between an activated terminal and its target cell. This mechanism of synapse duplication maintains specificity in information processing and provides a framework for understanding the numerous *in vivo* experiments that have demonstrated an increase in synapse number and complexity of dendritic arborization following exposure to an enriched environment or learning paradigms^{25,26}. □

Methods

Culture preparation and stimulation

Experiments were performed on hippocampal organotypic cultures prepared as described²⁷ and maintained for 12 days in culture. LTP was induced using TBS, a pattern of five bursts of stimulation at 5 Hz, each burst composed of four pulses at 100 Hz, repeated twice at a 10-s interval. To relabel activated synapses at the end of the experiments, a second theta burst was re-applied to the same group of afferents 5 min before fixation¹.

Morphological analyses

Slices were fixed for electron microscopy as described¹. Serial sections (ultratome Ultracut-E, Reichert-Jung) were stained *en bloc* first with 0.5% uranyl acetate in H₂O (pH 3.9) for 20 min before dehydration, then with 30 min of 2% uranyl acetate in ethanol after dehydration. Five to six sections per culture were usually examined with a Philips CM10 electron microscope at 80 kV. Synapses were randomly photographed at a magnification of 28,500× in an area corresponding to the middle portion of the apical arborization of CA1 pyramidal neurons. Images were digitized and dendritic spine profiles were classified blind by at least two independent observers as either labelled or unlabelled using as criteria the presence of accumulated electron-dense calcium precipitates in the spine head profile. In addition, we determined by densitometry the area of precipitate per spine profile (precipitate density; Fig. 1c). The results of the analyses made by the two observers and by densitometry agreed, with the exception of a small number of profiles (1–2%) that were discarded from quantitative analyses (white column, Fig. 1c). Synapses were identified by the presence of a definite postsynaptic membrane thickening and at least three presynaptic vesicles. Perforated synapses were identified by the presence of a discontinuity in the PSD and multiple spine boutons by the presence of at least two separate dendritic spines contacting the same presynaptic bouton. For three-dimensional analyses, ribbons of up to 60 serial sections were cut from each culture. Synaptic profiles corresponding to multiple spine boutons in which spines were clearly labelled or unlabelled were identified on the test section and then photographed serially at a magnification of at least 16,000×. For each slice culture, 3–13 labelled or unlabelled multiple spine boutons were reconstructed and the proportion of boutons in which the two spines arose from the same dendrite was calculated. For the stereological part of the study, the disector procedure was carried out as described²⁸. The proportion of labelled perforated synapses and multiple spine boutons was determined by systematic random sampling on six disector pairs in each block, using calcium precipitate as the counting unit.

All results are presented as mean \pm s.e.m., with *n* indicating the number of slice cultures analysed. Statistical analyses were carried out using Student's *t*-test or the Mann–Whitney test.

Received 10 September; accepted 6 October 1999.

- Calverley, R. K. & Jones, D. G. Contributions of dendritic spines and perforated synapses to synaptic plasticity. *Brain Res. Brain Res. Rev.* **15**, 215–249 (1990).
- Geinisman, Y., Detolledo-Morrell, L. & Morrell, F. Induction of long-term potentiation is associated with an increase in the number of axospinous synapses with segmented postsynaptic densities. *Brain Res.* **566**, 77–88 (1991).
- Geinisman, Y. *et al.* Structural synaptic correlate of long-term potentiation: formation of axospinous synapses with multiple, completely partitioned transmission zones. *Hippocampus* **3**, 435–445 (1993).
- Buchs, P. A. & Muller, D. Induction of long-term potentiation is associated with major ultrastructural changes of activated synapses. *Proc. Natl. Acad. Sci. USA* **93**, 8040–8045 (1996).
- Geinisman, Y., Detolledo-Morrell, L., Morrell, F., Persina, I. S. & Beatty, M. A. Synapse restructuring associated with the maintenance phase of hippocampal long-term potentiation. *J. Comp. Neurol.* **368**, 413–423 (1996).
- Bolshakov, V. Y., Golan, H., Kandel, E. R. & Siegelbaum, S. A. Recruitment of new sites of synaptic transmission during the cAMP-dependent late phase of LTP at CA3-CA1 synapses in the hippocampus. *Neuron* **19**, 635–651 (1997).
- Maletic-Savatic, M., Malinow, R. & Svoboda, K. Rapid dendritic morphogenesis in CA1 hippocampal dendrites induced by synaptic activity. *Science* **283**, 1923–1927 (1999).
- Engert, F. & Bonhoeffer, T. Dendritic spine changes associated with hippocampal long-term synaptic plasticity. *Nature* **399**, 66–70 (1999).
- Bliss, T. V. & Collingridge, G. L. A synaptic model of memory: long-term potentiation in the hippocampus. *Nature* **361**, 31–39 (1993).
- Sorra, K. E., Fiala, J. C. & Harris, K. M. Critical assessment of the involvement of perforations, spinules, and spine branching in hippocampal synapse formation. *J. Comp. Neurol.* **398**, 225–240 (1998).

11. Buchs, P. A., Stoppini, L., Parducz, A., Siklos, L. & Muller, D. A new cytochemical method for the ultrastructural localization of calcium in the central nervous system. *J. Neurosci. Methods* **54**, 83–93 (1994).
12. Sorra, K. E. & Harris, K. M. Occurrence and three-dimensional structure of multiple synapses between individual radiatum axons and their target pyramidal cells in hippocampal area CA1. *J. Neurosci.* **13**, 3736–3748 (1993).
13. Spacek, J. & Harris, K. M. Three-dimensional organization of smooth endoplasmic reticulum in hippocampal CA1 dendrites and dendritic spines of the immature and mature rat. *J. Neurosci.* **17**, 190–203 (1997).
14. McKinney, R. A., Capogna, M., Durr, R., Gähwiler, B. H. & Thompson, S. M. Miniature synaptic events maintain dendritic spines via AMPA receptor activation. *Nature Neurosci.* **2**, 44–49 (1999).
15. Fiala, J. C., Feinberg, M., Popov, V. & Harris, K. M. Synaptogenesis via dendritic filopodia in developing hippocampal area CA1. *J. Neurosci.* **18**, 8900–8911 (1998).
16. Ziv, N. E. & Smith, S. J. Evidence for a role of dendritic filopodia in synaptogenesis and spine formation. *Neuron* **17**, 91–102 (1996).
17. Trommald, M. & Hulleberg, G. Dimensions and density of dendritic spines from rat dentate granule cells based on reconstructions from serial electron micrographs. *J. Comp. Neurol.* **377**, 15–28 (1997).
18. Carlin, R. K. & Siekevitz, P. Plasticity in the central nervous system: do synapses divide? *Proc. Natl Acad. Sci. USA* **80**, 3517–3521 (1983).
19. Nieto-Sampedro, M., Hoff, S. F. & Cotman, C. W. Perforated postsynaptic densities: probable intermediates in synapse turnover. *Proc. Natl Acad. Sci. USA* **79**, 5718–5722 (1982).
20. Fischer, M., Kaech, S., Knutti, D. & Matus, A. Rapid actin-based plasticity in dendritic spines. *Neuron* **20**, 847–854 (1998).
21. Shi, S. H. *et al.* Rapid spine delivery and redistribution of AMPA receptors after synaptic NMDA receptor activation. *Science* **284**, 1811–1816 (1999).
22. Liao, D., Zhang, X., O'Brien, R., Ehlers, M. D. & Huganir, R. L. Regulation of morphological postsynaptic silent synapses in developing hippocampal neurons. *Nature Neurosci.* **2**, 37–43 (1999).
23. Woolley, C. S., Wenzel, H. J. & Schwartzkroin, P. A. Estradiol increases the frequency of multiple synapse boutons in the hippocampal CA1 region of the adult female rat. *J. Comp. Neurol.* **373**, 108–117 (1996).
24. Kirov, S. A., Sorra, K. E. & Harris, K. M. Slices have more synapses than perfusion-fixed hippocampus from both young and mature rats. *J. Neurosci.* **19**, 2876–2886 (1999).
25. Moser, M. B., Trommald, M. & Andersen, P. An increase in dendritic spine density on hippocampal CA1 pyramidal cells following spatial learning in adult rats suggests the formation of new synapses. *Proc. Natl Acad. Sci. USA* **91**, 12673–12675 (1994).
26. Kleim, J. A., Vij, K., Ballard, D. H. & Greenough, W. T. Learning-dependent synaptic modifications in the cerebellar cortex of the adult rat persists for at least four weeks. *J. Neurosci.* **17**, 717–721 (1997).
27. Stoppini, L., Buchs, P. A. & Muller, D. A simple method for organotypic cultures of nervous tissue. *J. Neurosci. Methods* **37**, 173–182 (1991).
28. Sterio, D. C. The unbiased estimation of number and sizes of arbitrary particles using the disector. *J. Microsc.* **134**, 127–136 (1984).

Acknowledgements

We thank L. M. Cruz-Orive for advice on stereology; K. Harris for 3D reconstruction software; D. Smithies for morphometry software on AVS; L. Parisi and M. Moosmayer for culture preparation and technical assistance; and F. Pillonel for photographic work. This work was supported by the Swiss National Science Foundation, the Human Frontier Science Program, the National Priority Program and the Jean-Falk Vairant Foundation.

Correspondence and requests for materials should be addressed to D.M. (e-mail: Dominique.Muller@medecine.unige.ch).

Conserved regulation of proximodistal limb axis development by Meis1/Hth

Nadia Mercader*, **Esther Leonardo***, **Natalia Azpiazu†**, **Antonio Serrano***, **Ginés Morata†**, **Carlos Martínez-A*** & **Miguel Torres***

* *Departamento de Inmunología y Oncología, Centro Nacional de Biotecnología, CSIC-UAM, E-28049 Madrid, Spain*

† *Centro de Biología Molecular, CSIC-UAM, Universidad Autónoma de Madrid, E-28049, Madrid, Spain*

Vertebrate limbs grow out from the flanks of embryos, with their main axis extending proximodistally from the trunk. Distinct limb domains, each with specific traits, are generated in a proximal-to-distal sequence during development¹. Diffusible factors expressed from signalling centres promote the outgrowth of limbs and specify their dorsoventral and anteroposterior axes^{2–4}. However, the molecular mechanism by which limb cells acquire

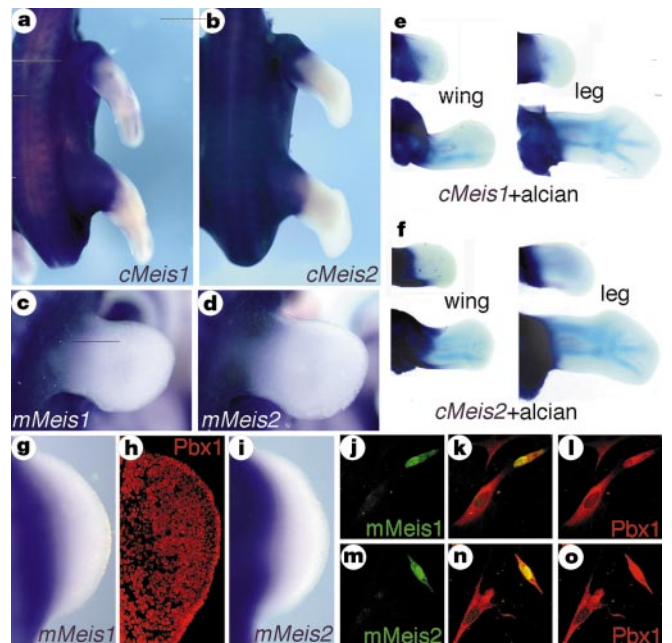


Figure 1 Coordinated *Meis/Pbx* expression in the limb bud. Whole-mount *in situ* hybridization (ISH) shows the expression of *cMeis1* (a), *cMeis2* (b), *mMeis1* (c) and *mMeis2* (d) in St. 29 chicken and embryonic day (E) 11.5 mouse limbs, respectively. Double alcian blue and ISH show the limits of *cMeis1* (e) and *cMeis2* (f) expression, together with chondrogenic condensations, between St. 23 and 28 of wing and leg development. **g–i**, Comparison of the expression domains of *mMeis1* (g) and *mMeis2* (i) messenger RNA with the nuclear domain of *Pbx1* (h). Endogenous *Pbx1* localization in mouse NIH 3T3 fibroblasts is shown in red (l, o) and HA-epitope detection denoting the presence and subcellular localization of Meis1 and Meis2 is shown in green (j, m). Co-localization of both proteins in the nucleus is shown in yellow (k, n).

their proximodistal (P–D) identity is unknown¹. Here we describe the role of the homeobox genes *Meis1/2* and *Pbx1* in the development of mouse, chicken and *Drosophila* limbs. We find that *Meis1/2* expression is restricted to a proximal domain, coincident with the previously reported domain in which *Pbx1* is localized to the nucleus⁵, and resembling the distribution of the *Drosophila* homologues *homothorax* (*hth*)^{5,6} and *extradenticle* (*exd*)⁷; that *Meis1* regulates *Pbx1* activity by promoting nuclear import of the *Pbx1* protein; and that ectopic expression of *Meis1* in chicken and *hth* in *Drosophila* disrupts distal limb development and induces distal-to-proximal transformations. We suggest that restriction of *Meis1/Hth* to proximal regions of the vertebrate and insect limb is essential to specify cell fates and differentiation patterns along the P–D axis of the limb.

Three distinct regions develop in a proximal-to-distal sequence along the vertebrate main limb axis; the stylopod (upper extremity), the zeugopod (lower extremity) and the autopod (hand or foot). The apical ectodermal ridge (AER), a specialized structure at the distal limb bud, and the zone of polarizing activity (ZPA), immediately posterior to the AER, produce signals that induce proliferation of progress zone cells, thereby promoting the growth of the limb bud and the generation of its main axis. Diffusible factors of the fibroblast growth factor (FGF) family emanating from the AER, and Sonic hedgehog from the ZPA, mediate the roles of these structures in P–D limb growth^{2,3}. Progress zone cells are stimulated by AER signalling to proliferate and generate the P–D limb axis by sequentially contributing progressively more distalized cells⁸.

We have studied the role of homeobox-containing genes showing conserved expression in specific P–D limb domains. Two highly related genes, *mMeis1* (refs 9, 10) and *mMeis2* (refs 11, 12), and the *Drosophila* orthologue *hth*⁶, are expressed in proximal domains of the limb primordium (Fig. 1c, d). To study the conservation of *Meis*